Water Mass Analysis of Effect of Climate Change on Air–Sea CO2 Fluxes: The Southern Ocean

Roland Séférian, Daniele Iudicone, Laurent Bopp, Tilla Roy, Gurvan Madec

Water Mass Analysis of Effect of Climate Change on Air–Sea CO_2 Fluxes: The Southern Ocean

ROLAND SÉFÉRIAN

LSCE/IPSL, Paris, France, and CNRM–GAME, Météo-France, CNRS, Toulouse, France

DANIELE IUDICONE

Stazione Zoologica Anton Dohrn, Naples, Italy

LAURENT BOPP AND TILLA ROY

LSCE/IPSL, Paris, France

GURVAN MADEC

IPSL/LOCEAN, Paris, France, and NOC, Southampton, United Kingdom

(Manuscript received 23 May 2011, in final form 22 November 2011)

ABSTRACT

Impacts of climate change on air–sea CO_2 exchange are strongly region dependent, particularly in the Southern Ocean. Yet, in the Southern Ocean the role of water masses in the uptake of anthropogenic carbon is still debated. Here, a methodology is applied that tracks the carbon flux of each Southern Ocean water mass in response to climate change. A global marine biogeochemical model was coupled to a climate model, making 140-yr Coupled Model Intercomparison Project phase 5 (CMIP5)-type simulations, where atmospheric CO_2 increased by 1% yr^{-1} to 4 times the preindustrial concentration ($4 \times CO_2$). Impacts of atmospheric CO_2 (carbon-induced sensitivity) and climate change (climate-induced sensitivity) on the water mass carbon fluxes have been isolated performing two sensitivity simulations. In the first simulation, the atmospheric CO_2 influences solely the marine carbon cycle, while in the second simulation, it influences both the marine carbon cycle and earth's climate. At $4 \times CO_2$, the cumulative carbon uptake by the Southern Ocean reaches 278 PgC, 53% of which is taken up by modal and intermediate water masses. The carbon-induced and climate-induced sensitivities vary significantly between the water masses. The carbon-induced sensitivities enhance the carbon uptake of the water masses, particularly for the denser classes. But, enhancement strongly depends on the water mass structure. The climate-induced sensitivities either strengthen or weaken the carbon uptake and are influenced by local processes through changes in CO_2 solubility and stratification, and by large-scale changes in outcrop surface (OS) areas. Changes in OS areas account for 45% of the climate-induced reduction in the Southern Ocean carbon uptake and are a key factor in understanding the future carbon uptake of the Southern Ocean.

1. Introduction

The Southern Ocean is a key component of the climate system. Its circulation is dominated by the Antarctic Circumpolar Current (ACC), which redistributes water masses between the Atlantic, Indian, and Pacific basins and plays a key role in the ocean general circulation (Sloyan and Rintoul 2001) and the global carbon cycle (Lovenduski et al. 2008; Marinov et al. 2008a,b). The global ocean takes up about one-quarter of the total anthropogenic emissions of CO_2 (i.e., 2.2 PgC yr^{-1} averaged over 1990–2009) (Le Quéré et al. 2009). The Southern Ocean (south of 30°S) is responsible for up to about 40% of the global oceanic CO_2 storage (Sabine et al. 2004).

Understanding the future evolution of oceanic carbon sink is difficult because it responds to a complex

Corresponding author address: Roland Séférian, Laboratoire des Sciences du Climat et de L'Environnement, Bâtiment 712, F-91191 Gif sur Yvette CEDEX, France.
E-mail: roland.seferian@lsce.ipsl.fr

DOI: 10.1175/JCLI-D-11-00291.1

interplay of processes. For example, increasing atmospheric p_{CO_2} leads to an increase in oceanic CO_2 uptake (a geochemical response), while the subsequent sea surface warming reduces the solubility of CO_2 and leads to a decrease in uptake (a climate response). To isolate these different carbon cycle responses, Friedlingstein et al. (2003) linearly separated the climate carbon cycle feedbacks into a geochemical sensitivity, which is a measure of the ocean's ability to uptake CO_2 in response to increasing atmospheric p_{CO_2}, and a climate sensitivity, which is a measure of the ocean's ability to uptake CO_2 in response to the evolution of global temperature.

Recently, some authors (e.g., Yoshikawa et al. 2008; Tjiputra et al. 2010; Roy et al. 2011) have shown that strong regional differences exist in the strength and sign of both geochemical and climate sensitivities, particularly in the Southern Ocean. There, the carbon uptake between 30° and 50°S is weakened due to climate change impacts, while south of 50°S it is strengthened. However, attribution of the processes driving these responses can be difficult if using regions with fixed geographical boundaries (i.e., latitudinal and longitudinal) because they do not necessarily coincide with the ''true'' boundaries that delimit regions with distinct air–sea CO_2 flux behavior.

It has long been known that there is a tight association between marine biogeochemical dynamics and the dynamics of the ocean. This association has been fruitful for both physical and biogeochemical studies, as clearly demonstrated by the pioneer work of Broecker (1991), which describes the meridional circulation of the global ocean using radioactive biogeochemical tracers.

Equally strong associations exist between the ocean dynamics, the water mass structure of the ocean, and the marine carbon cycle. It has been shown that the oceanic transport and cumulative carbon fluxes of carbon are tightly linked to water masses of the Southern Ocean (e.g., Sabine et al. 2004; Iudicone et al. 2011). In the Southern Ocean, the interplay between ocean dynamics and biogeochemistry is particularly strong, because it occurs where many of the key global water masses are formed [e.g., Southern Antarctic Modal Water (SAMW), Antarctic Intermediate Water (AAIW), and Antarctic Bottom Water (AABW)], are intensively modified [e.g., North Atlantic Deep Water (NADW)], or are simply redistributed among the main ocean basins with a considerable impact on the global carbon and nutrient cycles (e.g., Sarmiento et al. 2004; Sarmiento and Gruber 2006; Iudicone et al. 2011).

The idea to link hydrodynamic boundaries and the location of coherent air–sea CO_2 exchange is not a new concept. Recent observations (González-Dávila et al. 2011; Barbero et al. 2011) have shown that water masses often delineate the boundaries of CO_2 ingassing or outgassing regions. This is mainly because the air–sea CO_2 fluxes are modulated by the kinetic adjustment of the ocean–atmosphere p_{CO_2} disequilibrium, Δp_{CO_2} (e.g., Murnane et al. 1999; Sarmiento et al. 2000). Specifically, in the subtropics, the disequilibrium of p_{CO_2} between the ocean and the atmosphere is small because water masses are in direct contact with the atmosphere exchanging CO_2 over a longer period; here, the air–sea flux of CO_2 is mainly driven by the seasonal cycle and the variability of the atmospheric forcing. In contrast, south of 50°S, water masses have been isolated from the atmosphere for a long period, enhancing their Δp_{CO_2}; here, the flux is mainly driven by the Δp_{CO_2} itself.

In the context of climate change, several authors have demonstrated that ocean dynamics is impacted by changes in the pattern of westerly winds (e.g., Böning et al. 2008) and stratification, which induce changes in the structure, pattern, and properties of the water masses (e.g., Downes et al. 2009). However, it is not clear whether these water mass changes can lead to change in Southern Ocean carbon uptake.

We use simulations of a coupled carbon–climate model to investigate the impact of climate change on the oceanic carbon cycle within a water mass framework following the Iudicone et al. (2011) methodology. In a water mass framework, the carbon budgets are evaluated by partitioning the ocean into subregions using the ocean's natural coordinates (such as temperature, salinity, or density) instead of the more common geographical boundaries (e.g., latitude), which provides a more consistent association between the ocean dynamics and the biogeochemical dynamics.

In section 2, we briefly describe the model we use and the design of sensitivity experiments and we present and evaluate the water mass framework approach. Main results are described in section 3, where we focus on air–sea CO_2 fluxes and climate and carbon feedbacks. This is followed by the discussion in section 4.

2. Methodology

a. Experimental design

Climate-induced changes in ocean physics are simulated using the L'Institut Pierre-Simon Laplace Coupled Model, version 5 (IPSL CM5). The previous version of this coupled model, IPSL CM4, has been described by Marti et al. (2010). As part of the Coupled Model Intercomparison Project phase 5 (CMIP5) (Taylor et al. 2012), the IPSL CM5 climate model was integrated for 140 yr, starting from preindustrial conditions (CO_2 concentrations set to 284.7 ppm) and using a 1% per year increase in CO_2, reaching $4 \times CO_2$ after 140 yr. Monthly-mean outputs from the climate simulation were then

TABLE 1. Definition of the mean preindustrial water masses: the neutral density classes of the water masses (published by Sloyan and Rintoul 2001) and those of the simulated water masses, the annual mean of OS_{wm} (10^6 km^2 $\equiv$ 10^{12} m^2), annual mean V_{wm} (0^6 km^3 $\equiv$ 10^{15} m^3), annual mean SST (°C), and annual mean water mass CO_3^{2-} (μmol L^{-1}) for the generic water masses: TW and TMW, which can be considered as surface and subsurface water masses, respectively; MW and IW; and DW (e.g., NADW or CDW) and BW (e.g., AABW). Standard deviation of the surface temperature, CO_3^{2-}, the OS area, and V_{wm} are in parentheses.

Water mass	TW	TMW	MW	IW	DW	BW
Observed density classes	min–26.0	26.0–26.5	26.5–27.2	27.2–27.8	27.8–28.2	28.2–max
Simulated density classes	min–26.2	26.2–26.6	26.6–27.2	27.2–27.8	27.8–28.1	28.1–max
OS_{wm}	11.15 (0.85)	12.63 (1.0)	36.03 (1.55)	27.95 (1.35)	16.99 (1.29)	5.76 (1.34)
V_{wm}	2.09 (0.14)	4.14 (0.23)	29.78 (0.46)	77.38 (0.41)	266.48 (3.36)	58.38 (3.33)
SST	14.7 (3)	12.5 (2.3)	7.4 (3)	1.3 (2)	−1.6 (0.4)	−1.7 (0.1)
CO_3^{2-}	234.14 (22.7)	216.5 (21.1)	173.9 (23.2)	133.0 (11.1)	117.3 (6.1)	108.0 (8.5)

used to drive an offline version of our ocean biogeochemical general circulation model Nucleus for European Modelling of the Ocean (NEMO) Pelagic Interaction Scheme for Carbon and Ecosystem Studies (PISCES) (Aumont and Bopp 2006), in the ORCA2 configuration (Madec 2008), with a $2° \times 2° \cos(\phi)$ horizontal resolution and 31 vertical levels. Lateral mixing is evaluated along isoneutral surfaces. The model is supplemented with the Gent and McWilliams (1990) parameterization. The lateral mixing coefficient depends on the baroclinic instability growth rate (Treguier et al. 1997). The vertical mixing scheme uses a turbulent closure (Blanke and Delecluse 1993), and there is a diffusive bottom boundary layer parameterization (Beckmann and Döscher 1997). The model background vertical diffusivity increases from the surface to the bottom to mimic the effects of decreased stratification and increased small-scale turbulence near the bottom (values range from 0.12×10^4 m^2 s^{-1} in the first 1000 m to 1.2×10^4 m^2 s^{-1} at depth).

Three offline biogeochemical simulations have been carried out to isolate the response of the oceanic carbon cycle to rising atmospheric CO_2 concentrations from that due to climate change. All simulations start from the same preindustrial simulation that has been previously spun up for 3000 yr. In the first simulation, the control (CTRL), atmospheric CO_2 is fixed to its preindustrial value (i.e., 284.7 ppm). In the second simulation (GEOCLIM), climate change is induced by the anthropogenically induced increase in atmospheric CO_2. In the third simulation (GEO), only the increase in atmospheric CO_2 influences the oceanic carbon cycle; climate is kept at its preindustrial state.

b. *The water masses framework: Concept and evaluation*

To evaluate the yearly air–sea CO_2 fluxes and the climate carbon feedbacks (detailed in section 2c) in the Southern Ocean, we partitioned the domain using specific neutral density (ρ) ranges (Jackett and McDougall 1997) to classify the water masses (wms) following Sloyan and Rintoul (2001) and Iudicone et al. (2008). Neutral density classes are convenient for studying water masses, because neutral density classes conserve the same range of values for the whole water column. We have partitioned the Southern Ocean waters into thermocline water (TW), subtropical mode water (TWM), Subantarctic Mode Water (MW), Antarctic Intermediate Water (IW), deep water (DW, a class including mainly the circumpolar deep water (CDW) and thus also the modified NADW) and bottom water (BW, representing the Antarctic Bottom Water) (Table 1). Since the simulated water masses do not have the same density structures as observed, we select the water masses of the Southern Ocean to match the simulated to the observed physical and biogeochemical properties described in Sloyan and Rintoul (2001), Orsi et al. (1999), and Sørensen et al. (2001) (e.g., maximum or minimum of temperature, salinity, potential vorticity, currents, oxygen, and nitrate).

We define the water mass outcrop surface areas using the average locations of the outcropping isopycnal boundaries of each water mass over the winter (July–September). Winter is a natural context for studying the exchange between the ocean and the atmosphere, since the correspondence between surface and subsurface densities is maximal due to the strong vertical mixing.

The validity of the water mass framework can be appreciated from a comparison of surface fields with the isopycnals that delineate the regions where each water mass outcrops. The patterns of surface carbonate concentration (CO_3^{2-} in μmol L^{-1}; Table 1), sea surface temperature (SST in °C; Table 1; Fig. 2a), and dissolved inorganic carbon (DIC in μmol L^{-1}; Fig. 2b) match well with the pattern of the outcropping isopycnals of the water masses (Fig. 2). This means that the isopycnals of the water masses delineate the physical region where both the thermodynamical and the biogeochemical properties (e.g., SST and CO_3^{2-} or SST and DIC) are tightly linked. Also, both the patterns of the CO_2 fluxes (Fig. 2c) and their spatiotemporal variability (Fig. 2d)

are well aligned with the surface isopycnals of the outcropping water masses (further discussed in section 3). This indicates the importance of ocean dynamics in setting both the direction and the magnitude of the air–sea CO_2 exchange, and justifies using winter isopycnals to define the water masses.

c. Air–sea CO_2 and climate–carbon feedbacks

Here, we present the methodology for the analysis of air–sea CO_2 fluxes and the climate and geochemical feedbacks within a water mass framework. Water mass CO_2 uptake [$F_{wm}(t)$, PgC yr^{-1}] has been computed by integrating local annual air–sea CO_2 flux (gC m^{-2} yr^{-1}) over the outcrop surface area of each water mass (OS_{wm}) as follows:

$$F^i_{wm}(t) = \int_{OS_{wm}(t)} f^i_{OA}(t)\, dS, \quad \text{where} \quad \begin{cases} i \equiv (\text{CTRL, GEO, GEOCLIM}) \\ \text{wm} \equiv (\text{TW, TMW, MW, IW, DW, BW}) \end{cases}. \tag{1}$$

Note that negative water mass CO_2 fluxes correspond to an oceanic uptake of atmospheric CO_2.

We compute the water mass CO_2 uptake for the GEO simulations over the OS_{wm} of the water mass under preindustrial climate (OS^{GEO}_{wm}, m^2) and for the GEOCLIM simulation over the OS of the water mass under climate change ($OS^{GEOCLIM}_{wm}$, m^2). That is, $OS^{GEOCLIM}_{wm}(t) = OS^{GEO}_{wm}(t) + \Delta OS_{wm}(t)$, where $\Delta OS(t)$ (in m^2) is the change in OS_{wm} due to climate change.

The net cumulative water mass CO_2 flux is computed after correcting for the model drift and the mean preindustrial state using the CTRL simulation as follows:

$$\Delta C^{net}_{wm}(t) = \int_{t_0}^{t} [F^{GEOCLIM}_{wm}(\tau) - F^{CTRL}_{wm}(\tau)]\, d\tau. \tag{2}$$

Similarly, the geochemical component of the water mass CO_2 flux, due to rising atmospheric CO_2, under preindustrial climate in the GEO simulation [$\Delta C^{geo}_{wm}(t)$] is

$$\Delta C^{geo}_{wm}(t) = \int_{t_0}^{t} F^{GEO}_{wm}(\tau) - F^{CTRL}_{wm}(\tau)\, d\tau. \tag{3}$$

The evolution of the geochemical (carbon induced) sensitivity (β_{wm}, gC m^{-2} ppm^{-1}), due to the enhancement of air–sea exchange in response to increasing atmospheric CO_2 concentrations under a preindustrial climate, is

$$\beta_{wm}(t) = \frac{1}{p_{CO_2}(t) - p_{CO_2}(t_0)} \int_{t_0}^{t} \frac{F^{GEO}_{wm}(\tau) - F^{CTRL}_{wm}(\tau)}{OS^{GEO}_{wm}}\, d\tau. \tag{4}$$

To isolate the climate component of the water mass carbon CO_2 flux, $\Delta C^{clim}_{wm}(t)$, we have to remove the geochemical component of the water mass carbon CO_2 flux in the GEOCLIM simulation. This is not simply $\Delta C^{geo}_{wm}(t)$, because OS_{wm} (and the associated geochemically driven CO_2 flux) alters with climate change. The geochemical water mass CO_2 flux attributed to change in OS_{wm}, $F^{\Delta OS}_{wm}(t)$, is

$$F^{\Delta OS}_{wm}(t) = \beta_{wm}(t) \Delta p_{CO_2}(t)/\Delta t \Delta OS_{wm}(t), \tag{5}$$

where $\Delta p_{CO_2}(t)/\Delta t$ is the yearly evolution of p_{CO_2} in ppm yr^{-1}.

Therefore, the associated outcrop surface component of the cumulative water mass CO_2 flux is

$$\Delta C^{\Delta OS}_{wm}(t) = \int_{t_0}^{t} F^{\Delta OS}_{wm}(\tau)\, d\tau. \tag{6}$$

Thus, the climate component of the cumulative carbon fluxes for a given water mass due to climate change and not related to change in OS_{wm}, $\Delta C^{clim}_{wm}(t)$, is

$$\Delta C^{clim}_{wm}(t) = \int_{t_0}^{t} [F^{GEOCLIM}_{wm}(\tau) - F^{GEO}_{wm}(t) - F^{\Delta OS}_{wm}(\tau)]\, d\tau \tag{7}$$

and the evolution of the climate-driven sensitivity of the water mass (γ_{wm}, gC m^{-2} °C^{-1}),

$$\gamma_{wm}(t) = \frac{1}{T(t) - T(t_0)} \times \int_{t_0}^{t} \frac{F^{GEOCLIM}_{wm}(\tau) - F^{GEO}_{wm}(\tau) - F^{\Delta OS}_{wm}(\tau)}{OS^{GEOCLIM}_{wm}} d\tau, \tag{8}$$

can be determined, where T is the global mean atmospheric surface air temperature at 2 m.

The net cumulative CO_2 flux of each water mass can be reformulated as

$$\Delta C^{net}_{wm}(t) = \Delta C^{clim}_{wm}(t) + \Delta C^{geo}_{wm}(t) + \Delta C^{\Delta OS}_{wm}(t), \tag{9}$$

where $\Delta C^{geo}_{wm}(t)$ and $\Delta C^{\Delta OS}_{wm}(t)$ are due to changes in the local CO_2 fluxes within the water mass, driven by rising atmospheric CO_2 (i.e., geochemical processes), while $\Delta C^{clim}_{wm}(t)$ is due to changes in local CO_2 fluxes within the water mass, driven by climate change. However, it is important to note, that although $\Delta C^{\Delta OS}_{wm}(t)$ is locally driven by geochemical processes, it is a climate-induced component to the net cumulated CO_2 flux, because $\Delta OS_{wm}(t)$ is a response to climate change.

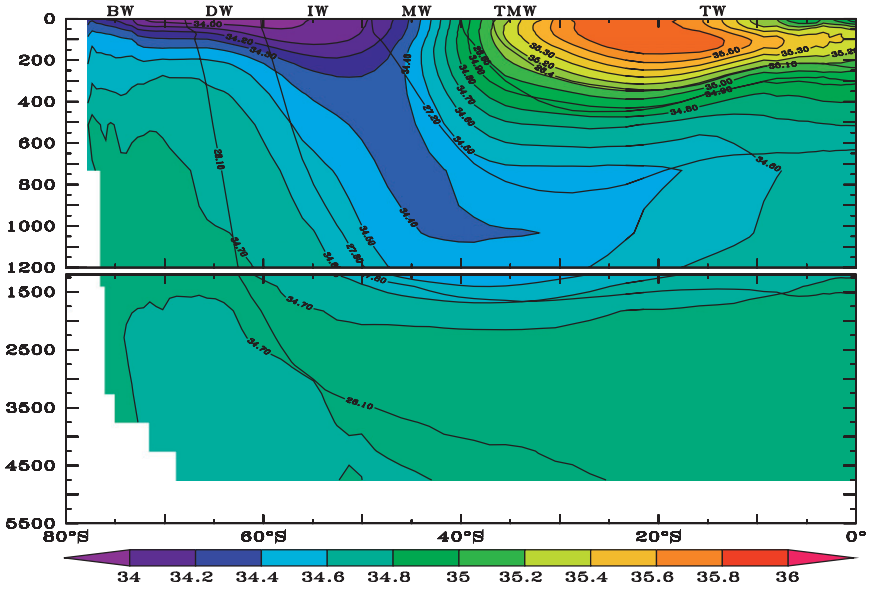

FIG. 1. Zonally averaged mean state seawater salinity from the preindustrial simulation of the IPSL CM5A. Superimposed lines correspond to the preindustrial mean-state-defined density classes (min, 26.2, 26.6, 27.2, 27.8, 28.1, max) for the TW, TMW, MW, IW, DW, and BW, respectively.

3. Results

a. *Preindustrial climate*

1) PREINDUSTRIAL WATER MASSES

Southern Ocean water masses are delineated by the density classes presented in Table 1 and Fig. 1. Even if interannual variability affects the location of the distinct water masses, TW and TMW are broadly located in the subtropics, modal and intermediate waters (MW and IW, respectively) in the midlatitudes, and DW and BW in subpolar–polar regions. In the preindustrial mean state, MW and IW occupy a large fraction of the Southern Ocean area (about 110.51×10^6 km^2), 33% and 25%, respectively. TW, TMW, DW and BW occupy 10%, 11%, 16%, and 5% respectively.

As we conduct idealized sensitivity simulations starting from a preindustrial climate state, it is difficult to quantitatively evaluate the water mass pattern, structure, and properties because preindustrial modeled water masses cannot be directly compared to modern observed water masses. Nevertheless, the characteristics of the modeled water masses seem to match with the characteristics of modern water masses described in the literature (e.g., Sloyan and Rintoul 2001; Jackett and McDougall 1997; Tomczak and Liefrink 2005): TW and TMW are warm and salty; MW is characterized by a large volume of water; IW and DW are characterized by a subsurface minimum salinity in subsurface and a salinity maximum at depth, respectively; and BW is cold and fresher.

2) PREINDUSTRIAL AIR–SEA CO_2 FLUXES

In the preindustrial state (CTRL simulation), the mean state of the Southern Ocean carbon uptake is about -0.06 ± 0.12 PgC yr^{-1}, meaning that the Southern Ocean is a weak net sink of carbon (Table 2). Hereafter, we propose a short evaluation of the modeled preindustrial carbon uptake using the only available product of preindustrial carbon fluxes estimated from ΔC^* and inversed modeling (Mikalhof-Fletcher et al. 2007). The regional carbon fluxes around our region of interest (<30°S) are about -0.60 PgC yr^{-1} in the midlatitudes (between 18° and 42°S), 0.17 PgC yr^{-1} in subpolar regions (between 42° and 60°S), and -0.10 PgC yr^{-1} south of 60°S, and are very comparable to the range of the model estimates of preindustrial regional carbon fluxes published by Mikalhof-Fletcher et al. (2007). Now, regarding the water mass carbon fluxes, we find that the

TABLE 2. Integrated [$F_{wm}(t)$, PgC yr^{-1}] air–sea CO_2 fluxes within the different water masses at $4 \times CO_2$ for the simulations GEO and GEOCLIM. These fluxes are computed according to Eq. (1). Convention: negative value means uptake of CO_2 from the atmosphere.

Water mass	TW	TMW	MW	IW	DW	BW	Southern Ocean
$F_{wm}^{CTRL}(t)$	−0.10	−0.07	−0.16	0.17	0.07	0.03	−0.06
$F_{wm}^{GEO}(t)$	−0.19	−0.18	−0.83	−1.29	−0.75	−0.19	−3.43
$F_{wm}^{GEOCLIM}(t)$	−0.68	−0.20	−0.48	−0.94	−0.70	−0.06	−3.06

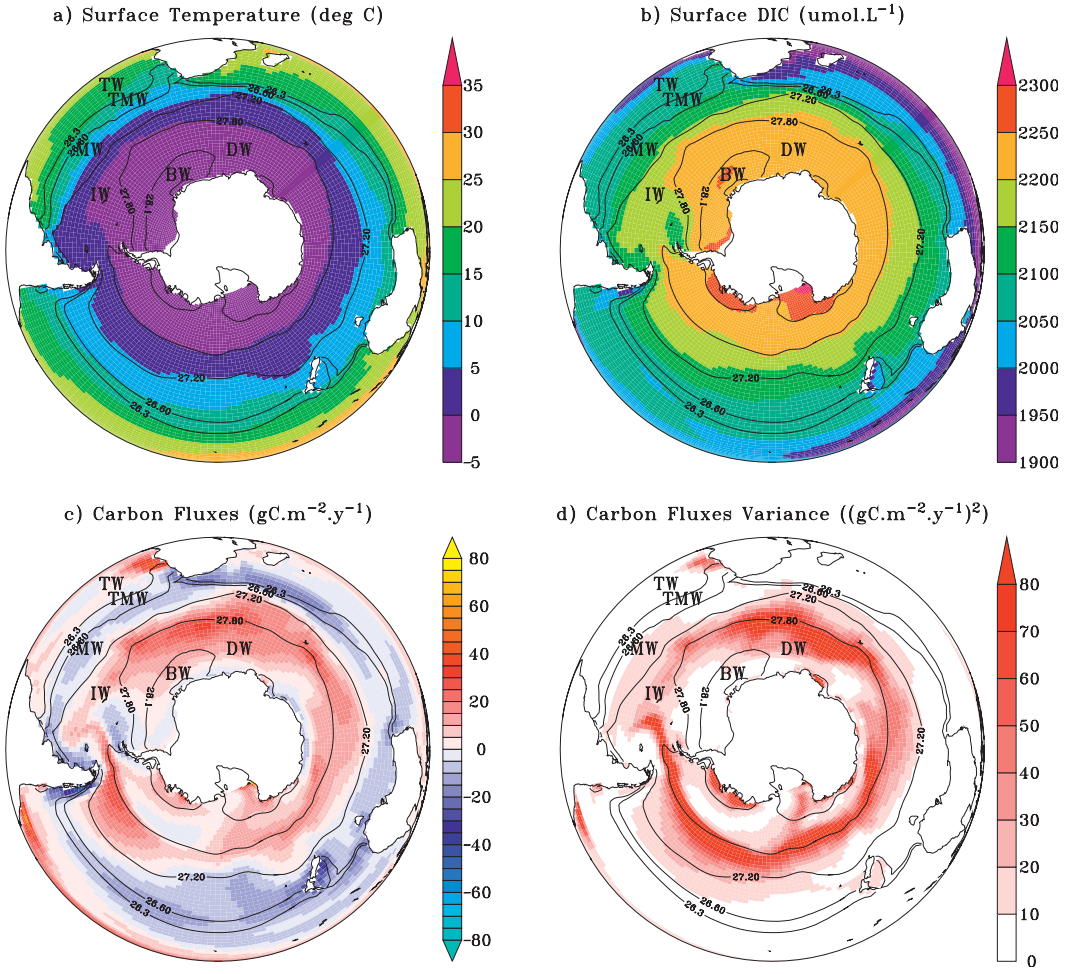

FIG. 2. Maps based on the preindustrial mean state simulation: (a) the SST (°C), (b) the surface concentrations of DIC (μmol L^{-1}), (c) the air–sea CO_2 exchange (gC m^{-2} yr^{-1}), and (d) the variance of the air–sea CO_2 exchange of the 140 yr from the preindustrial simulation. Superimposed contours represent the preindustrial mean state winter density classes of the defined water masses.

TW, TMW, and MW act as ingassing regions (Figs. 2 and 3a–c; Table 2). These surface water masses are in prolonged interaction with the atmosphere over the year, such that the activity of the soft-tissue pump during photosynthesis results in an net uptake of CO_2. The activity of the solubility pump within these water masses is strongly influenced by seasonal cycle: water masses take up carbon during winter and outgas carbon during summer (e.g., Sarmiento and Gruber 2006).

IW, DW, and BW act as outgassing regions (Fig. 3c; Table 2). The DW, which has been isolated from the atmosphere for a long period, contains high concentrations of dissolved inorganic carbon. Thus, when DW upwells, the p_{CO_2} of the DW is much greater than the p_{CO_2} of the atmosphere and drives a strong outgassing of CO_2. Since IW and BW are created from the surface recirculation and transformation of DW (e.g., Iudicone et al. 2011; Toggweiler et al. 2006; d'Orgeville et al. 2010), a strong outgassing also occurs where IW and BW are formed. Large carbon flux variability occurs at places where isopycnals delineate DW and IW (Fig. 2b). Places with high air–sea CO_2 flux variance correspond to regions where surface isopycnals of the outcropping water mass boundaries vary the most, because the surface isopycnals respond to ocean–atmosphere forcing (e.g., Lovenduski et al. 2008; Verdy et al. 2007; Lenton and Matear 2007; Lenton et al. 2009).

b. *Impacts of climate change*

1) CHANGE IN WATER MASS PATTERN AND STRUCTURE

Ocean warming, freshening (due to sea ice melting and precipitation), and stratification (Fig. 4) affect the

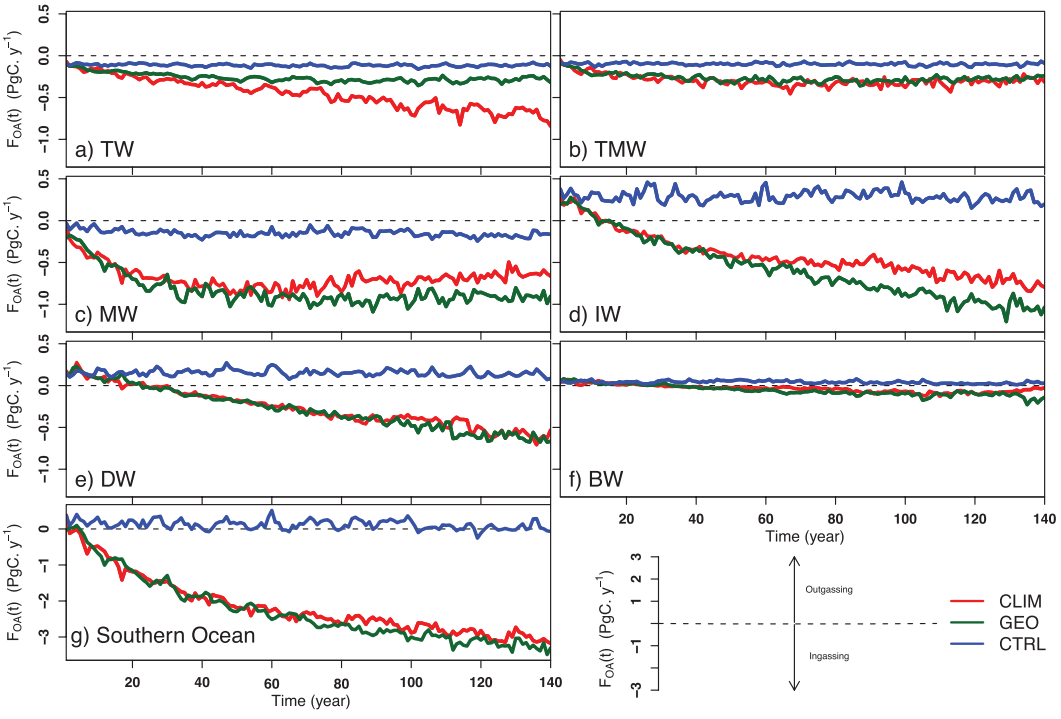

FIG. 3. Water mass uptake of CO_2 [F^i_{wm} (PgC yr^{-1}), where i = CTRL, GEO, or GEOCLIM; Eq. (1)] of (a) TW, (b) TMW, (c) MW, (d) IW, (e) DW, and (f) BW. (g) The carbon uptake of the Southern Ocean.

ocean density, causing change in the water mass pattern and structure (Figs. 5, 6). This change broadly reflects a southward shift of the water mass location and thus a change of the modeled water mass outcrop surface areas. Similar behavior has been found in previous studies (e.g., Downes et al. 2009).

At $4 \times CO_2$, OS_{TW} and OS_{TMW} increase, while OS_{MW}, OS_{IW}, OS_{DW} and OS_{BW} are reduced in response to climate change meaning that ocean surface warming and freshwater input have induced a reduction of water density (about 0.01 kg m^{-3}). Of the Southern Ocean area, the TW and TMW occupy about 44%, the MW and IW 42% and the DW and BW 13 and 1% respectively.

2) CHANGE IN NET WATER MASS CARBON UPTAKE

Water mass carbon uptake increases in response to rising atmospheric CO_2 (Fig. 3), meaning that all of the water masses take up carbon from the atmosphere. At $4 \times CO_2$, the net Southern Ocean carbon uptake changes significantly from its preindustrial value, reaching -3.06 PgC yr^{-1} (Table 2).

Over the 140-yr simulation, the net cumulative carbon uptake of the Southern Ocean [$\Delta C^{net}(t)$] reaches 278.2 PgC and is unequally partitioned between the distinct water masses (Fig. 7). MW and IW account for 25% and 27% of the Southern Ocean cumulative carbon uptake, respectively, meaning that MW and IW quantitatively dominate the cumulative anthropogenic carbon fluxes of the Southern Ocean.

A comparison between Fig. 3 and Fig. 5 highlights that, for some water masses, changes in carbon uptake and OS_{wm} are tightly linked. Indeed, the temporal correlation between carbon uptake and OS_{wm} for a given water mass can reach up to 0.92 for TW, 0.61 for IW, and 0.85 for DW (0.4 for the other water masses). This supports the fact that some of the greatest changes in water mass carbon uptake are a response to changes in their outcrop surface area.

c. *Components of the net water mass carbon uptake*

Under changing climate (GEOCLIM simulation), the ability of the Southern Ocean to take up CO_2 from the atmosphere is reduced by 10% at $4 \times CO_2$ relative to the simulation GEO (Table 2). The relative change in Southern Ocean carbon uptake differs between the water masses (Table 2). The impacts of rising atmospheric CO_2 and climate change on the net CO_2 flux of each water mass have been separated into the following three components [Fig. 7; Eq. (9)]:

- A geochemical component, ΔC^{geo}_{wm}, solely due to the contribution of rising atmospheric CO_2 in absence of climate change on the water mass carbon uptake [Eq. (3)].

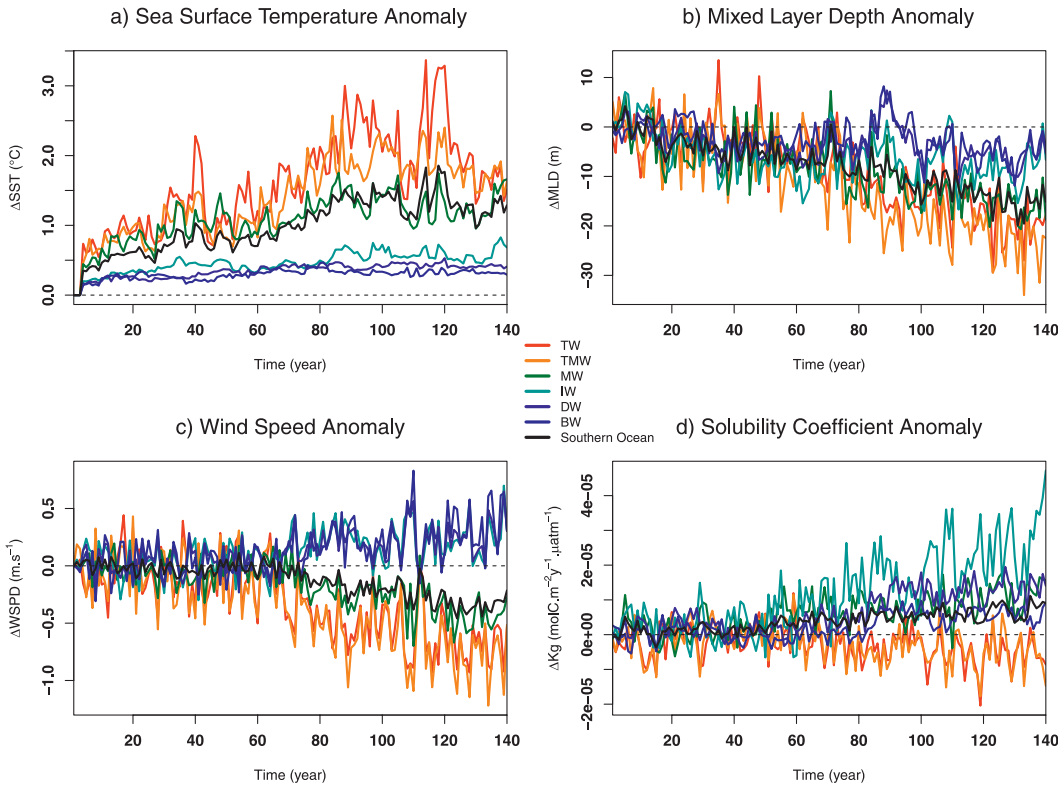

FIG. 4. Annual evolution of water-mass-averaged (a) surface temperature anomaly, (b) mixed layer depth anomaly, (c) wind speed anomaly, and (d) solubility coefficient anomaly computed between the simulations GEOCLIM and GEO.

- An outcrop surface component, $\Delta C_{wm}^{\Delta OS}$, due to the changes in the net geochemically driven carbon fluxes related to climate-driven changes in the outcrop surface areas of the water masses [Eq. (6)].
- A climate component, ΔC_{wm}^{clim}, due to the contribution of climate-driven changes in local processes (e.g., CO_2 solubility, stratification) controlling the water mass carbon uptake (Eq. (7)].

1) THE GEOCHEMICAL COMPONENT

The geochemical component, $\Delta C_{wm}^{geo}(t)$, is solely due to rising atmospheric CO_2 in the absence of climate change and corresponds to a net sink of carbon for all of the water masses. This implies that the Southern Ocean takes up atmospheric carbon as soon as the atmospheric p_{CO_2} increases (Fig. 3). However, we can clearly distinguish that the water masses exhibit two different CO_2 uptake behaviors in response to rising CO_2: the carbon uptake of TW, TMW, and MW exhibit a nonlinear saturation process, while that of IW, DW, and BW are linear.

These different responses are mainly due to changes in water mass carbon chemistry that are associated with the penetration of CO_2 into seawater. The saturation levels of the water mass carbon uptake appear to be related to the water mass volume (V_{wm}) but not to surface concentrations of CO_3^{2-} (Table 1). These results will be discussed in greater detail afterward.

Again, at 4 × CO_2, Fig. 7 shows that that $\Delta C_{MW}^{GEO}(t)$ and $\Delta C_{IW}^{GEO}(t)$ are stronger than the net cumulative uptake of the other water masses and account for 56% of the total Southern Ocean $\Delta C_{wm}^{GEO}(t)$ (298.3 PgC).

2) THE OUTCROP SURFACE COMPONENT

This component $\Delta C_{wm}^{\Delta OS}(t)$ is solely related to the modulation of the carbon-induced sensitivity due to change in OS_{wm} (Fig. 6). It results in a significant increase of $\Delta C_{TW}^{\Delta OS}(t)$, because the OS_{TW} increases (Fig. 5). The opposite phenomenon happens for MW and IW. As the OS_{MW} and OS_{IW} become smaller, this accounts for a significant reduction of MW and IW cumulative carbon uptake. Changes in OS_{wm} reduce the cumulative anthropogenic carbon uptake by 18.14 PgC, because the reduction of OS_{wm} affects mainly the water masses, which are the most highly responsive to rising CO_2 (Fig. 6).

3) THE CLIMATE COMPONENT

The climate component, $\Delta C_{wm}^{clim}(t)$, quantifies the local impact of climate change including the impacts of both

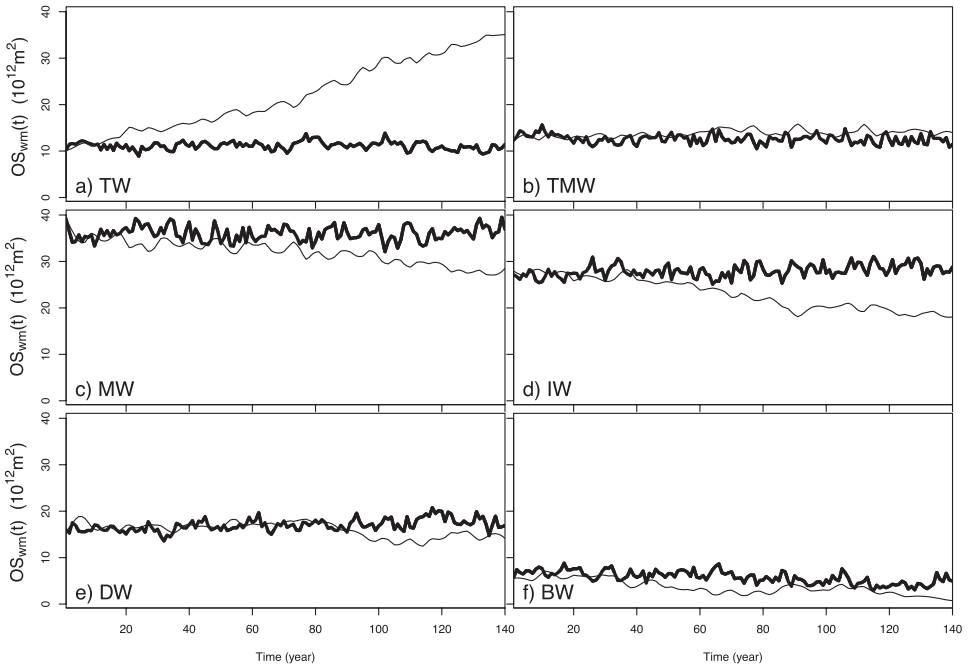

FIG. 5. Winter water mass OS (10^{12} m^2 $\equiv$ 10^6 km^2) area time series computed using a nonparametric loess smoothing. The bold lines correspond to the GEO simulation, whereas the thin lines correspond to the GEOCLIM simulation. Shown are the integrated air–sea CO_2 fluxes of the (a) TW, (b) TMW, (c) MW, (d) IW, (e) DW, and (f) BW.

change in CO_2 solubility due to modifications of temperature and salinity and change in vertical mixing, but not in OS_{wm}. This component is well documented in the literature (e.g., Roy et al. 2011; Crueger et al. 2008). But, the climate component in these studies cannot be directly compared with ours, because they calculated the combined influence of what we call $\Delta C_{wm}^{\Delta OS}(t)$ and $\Delta C_{wm}^{clim}(t)$. We find that the total Southern Ocean $\Delta C_{wm}^{clim}(t)$ induces a reduction of the Southern Ocean carbon uptake of about 2.39 PgC, which is much smaller than the values given by the previous studies (i.e., we attribute most to the change in OS_{wm}). Nevertheless, in the Southern Ocean, this small climate component results from an imbalance between the strong negative $\Delta C_{TW}^{clim}(t)$ and the strong positive $\Delta C_{IW}^{clim}(t)$, which cancel each other out (Fig. 6).

d. *Water mass carbon-induced and climate-induced sensitivities*

In this section, we determine the β_{wm} and the γ_{wm} of each water mass following the method applied in the linear feedback analysis of Friedlingstein et al. (2003).

As demonstrated in section 2 and Table 2, IW and DW are the principal drivers of the carbon-induced sensitivity in the Southern Ocean (Table 2). However, we

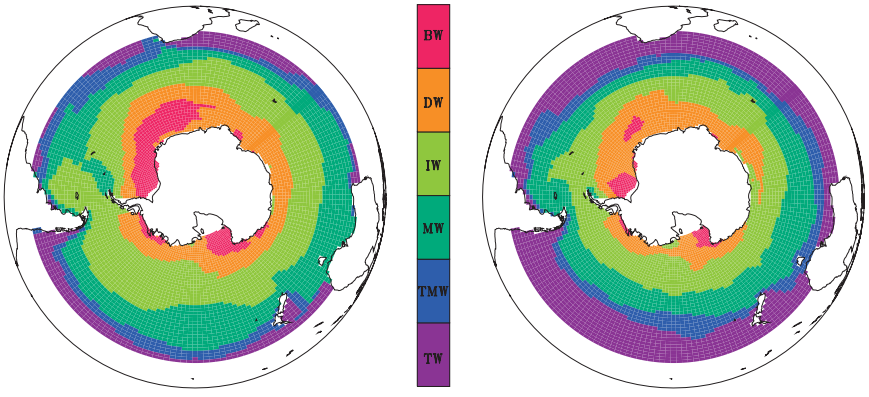

FIG. 6. The water mass pattern of (a) the preindustrial mean state (last 10 yr of GEO) and (b) the climate change mean state (last 10 yrs of GEOCLIM).

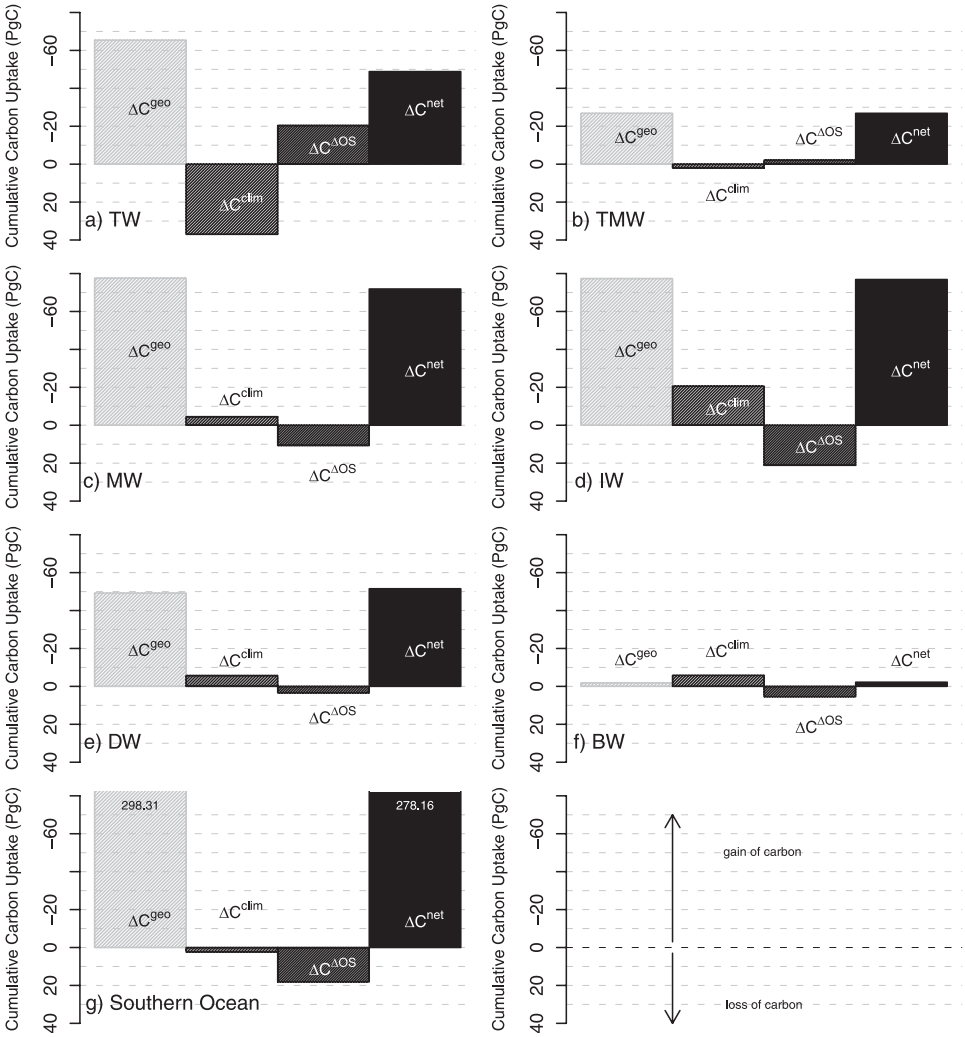

FIG. 7. The net cumulative carbon uptake, $\Delta C_{\mathrm{wm}}^{\mathrm{net}}$ [Eq. (2)] and its three components [$\Delta C_{\mathrm{wm}}^{\mathrm{geo}}$, $\Delta C_{\mathrm{wm}}^{\Delta\mathrm{OS}}$, and $\Delta C_{\mathrm{wm}}^{\mathrm{clim}}$ shown in Eqs. (3), (6), and (7)] for each water mass and for the Southern Ocean.

show that the time evolution of the carbon-induced sensitivity differs a great deal between the modeled water masses (Figs. 8a,b). The time evolution of the carbon-induced sensitivity mainly reflects the saturation process. The time evolution of β_{TW}, β_{TMW}, and β_{MW} modulate in turn the carbon-induced sensitivity of the Southern Ocean. It peaks at year 89 (i.e., 4.1 gC m^{-2} ppm^{-1}) and drops to 3.6 gC m^{-2} ppm^{-1} at $4 \times \mathrm{CO}_2$, indicating that the Southern Ocean carbon uptake could saturate under higher levels of atmospheric CO_2.

As for β_{wm}, γ_{wm} varies a great deal over time (Figs. 8c,d). At $4 \times \mathrm{CO}_2$, γ_{TW} controls the negative climate-induced sensitivity of the Southern Ocean (i.e., −4.15 gC m^{-2} $^{\circ}\mathrm{C}^{-1}$; Table 3). The sign of γ_{wm} associated with the location of the distinct water masses seems to correspond to the sign of climate-induced sensitivity published in previous regional climate sensitivities studies (e.g., Yoshikawa et al. 2008; Tjiputra et al. 2010; Roy et al. 2011): the climate-induced sensitivity induces a reduction of the ocean carbon uptake in the subtropics and a strengthening in the subpolar and polar regions.

4. Discussion

Our findings shed light on the strong dependency of the future Southern Ocean uptake of carbon on the evolution of water mass properties under a changing climate. Such a dependency has been suggested in recent literature (e.g., Lovenduski and Ito 2009; Tschumi et al. 2008). In these studies, the authors have demonstrated that changes in wind stress and stratification could cause not only change in isopycnal outcrop surface areas but also lead to a weaker Southern Ocean carbon uptake. However, these authors did not truly associate the

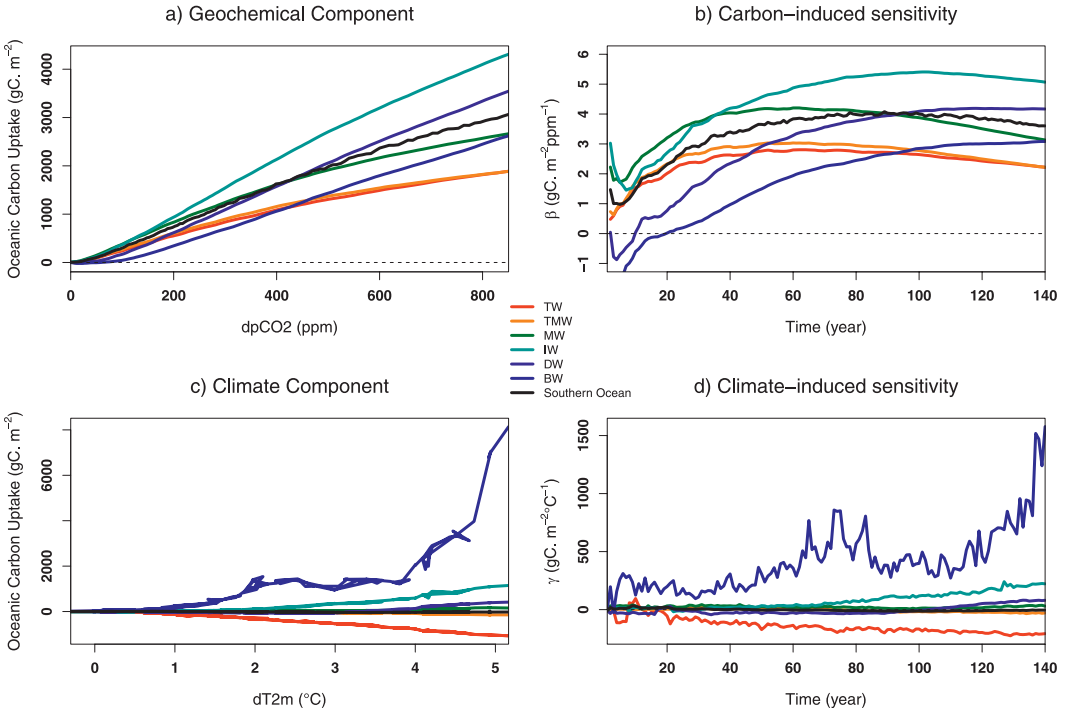

FIG. 8. The annual evolution the oceanic uptake of carbon due to (a) the carbon-induced component and (b), the climate-induced component. (left) The evolution of (c) β_{wm} and (d) γ_{wm} along the 140-yr time series for each water mass. Note that the interplay between the water mass net air–sea CO_2 uptake and the local impact of the global air surface temperature (T) is highly variable. As a consequence, the evolution of β_{wm} and γ_{wm} has been computed using a nonparametric loess smoothing.

weakening of the Southern Ocean carbon uptake with changes in water mass pattern. Here, we find that changes in the outcrop surface area of the Southern Ocean water masses [outcrop surface component; Eq. (6)] appear to be the primary fingerprint of climate change on water mass carbon uptake. Since the outcrop surface component weakens the carbon uptake of the dominant water mass (i.e., MW and IW), it results in a weakening of the Southern Ocean carbon uptake.

Nevertheless, previous model studies (e.g., Lenton et al. 2009; Crueger et al. 2008; Lovenduski and Ito 2009; Tschumi et al. 2008) or observation-based studies (e.g., Le Quéré et al. 2007) have also demonstrated that the Southern Ocean carbon uptake could be highly sensitive to change in wind pattern and stratification. The carbon uptake of the Southern Ocean is presumed to be linearly sensitive to changes in wind stress and nonlinearly sensitive to changes in stratification (Lovenduski and Ito 2009). Such linear or nonlinear carbon uptake behaviors have also been found in our results for the Southern Ocean water masses (Fig. 3). However, we find that the behaviors of linear or nonlinear carbon uptake are highly dependent on the water masses. The outcrop surface component appears to be significantly linear for TW, IW, and DW but to a lesser degree for the other water masses, while change in marine carbon chemistry, CO_2 solubility, and stratification can induce either a linear or a nonlinear behavior in the carbon uptake of the water masses.

Even in the absence of climate change, we find that the water mass carbon uptake can exhibit either a linear behavior for DW and BW or a nonlinear behavior for the other water masses in response to rising CO_2 [i.e., the geochemical component, Eq. (3)]. These different behaviors are driven by the marine carbon chemistry, because the buffering process of the penetration of CO_2 into seawater consumes surface CO_3^{2-} ($CO_2 + CO_3^{2-} + H_2O = 2HCO_3^-$). Of major concern, this buffering process, associated with the saturation of the water mass carbon uptake, modulates the geochemical component, which is the major driver of the Southern Ocean carbon uptake (Fig. 8).

TABLE 3. Sensitivities β_{wm} (gC m^{-2} ppm^{-1}) and γ_{wm} (gC m^{-2} °C^{-1}) at 4 × CO_2. They are computed according to Eqs. 3–and 5.

	TW	TMW	MW	IW	DW	BW	Southern Ocean
β_{wm}	2.22	2.22	3.13	5.07	4.17	3.08	3.60
γ_{wm}	−208.41	−30.14	33.72	223.73	79.02	1408.22	−4.15

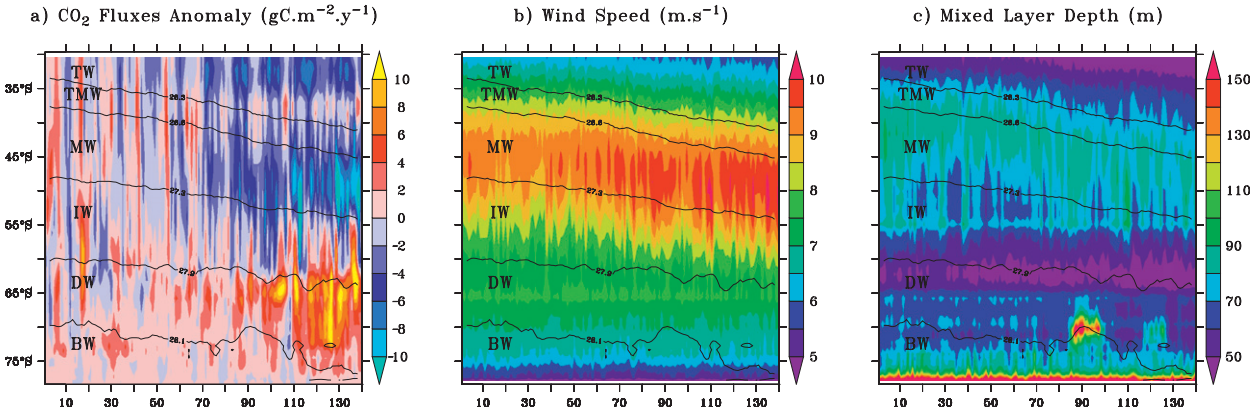

FIG. 9. Hovmöller diagram of (a) the air–sea CO_2 fluxes anomaly $[f_{OA}^{GEOCLIM}(t) - f_{OA}^{GEO}(t)]$ (gC m^{-2} yr^{-1}), (b) the annual Southern Ocean wind speed at 10 m (m s^{-1}), and (c) the mixed layer depth (m) along the 140 yr of the GEOCLIM simulation.

When CO_2 is taken up from the atmosphere, its dissolution into seawater induces a consumption of CO_3^{2-}. Without a replenishing process, which brings a CO_3^{2-} ion from subsurface waters to the surface, a saturation of the atmospheric CO_2 sink appears within water masses. Usually, CO_3^{2-} surface concentration is controlled at first by temperature (Table 1). This should priori lead to a faster saturation of the colder water masses (i.e., IW, DW, and BW). However, the opposite phenomenon occurs. Our analysis shows that the saturation of the water mass carbon uptake appears to be more influenced by the total amount of CO_3^{2-} available in the water mass [linked to V_{wm}; Table 1] than the surface concentration of CO_3^{2-}. Vertical mixing due to the intense frontal zone, such as the ACC, make the deep amount of CO_3^{2-} replenish the surface CO_3^{2-} consumed due to the buffering process.

The trends of the water mass uptake of CO_2 and the resulting carbon-induced sensitivity shed light on the nonlinear time dependency of the supply mechanism. The shift of water mass carbon uptake regime and the water mass carbon-induced sensitivity, which occurs at different times for the various water masses, are strongly linked to the mixing time needed for buffering the penetration of the atmospheric p_{CO_2} into seawater. Surface depth interconnections, the rate of deep water formation, and the winter mixing intensity in the Southern Ocean control a part of CO_2 absorption at the surface and strongly impact the atmospheric p_{CO_2}.

Under a changing climate, our results show that changes in wind pattern or mixed layer depth do not cause a southward shift of the outcrop surface area of the water masses, because the southward shift of the outcrop isopycnals occurs slightly faster that the southward shift of the westerly winds (Fig. 9). This is mainly because the ocean warming induces a direct change in seawater density. These changes in surface temperature and wind pattern induce a small and linear change in CO_2 solubility over the subtropical water masses (TW, TMW), and have strong implications on water masses influenced by ice cover (BW) or the regions directly impacted by the strengthening of the westerlies (IW) (Fig. 4). Notably, the changes in the mixed layer depth due to stratification can amplify the nonlinear saturation process discussed above. However, a reduction of mixed layer depth does not necessarily imply a buildup of CO_2 in the water mass subsurface waters. Several hypotheses can be drawn: 1) ocean carbon fluxes and carbon storage are disconnected (e.g., Marinov and Gnanadesikan 2011); and 2) processes like advection, the exchange of carbon across isopycnals, and diffusion can possibly contribute to a large part of the carbon stored in the water mass (e.g., Iudicone et al. 2011).

These possible physical mechanisms have been attributed to large-scale changes in water mass pattern and structure, which contribute significantly to the modulation of the carbon uptake and agree with the findings of Lovenduski and Ito (2009) and Tschumi et al. (2008). However, we acknowledge that these mechanisms have been addressed with a coarse-resolution model. Therefore, our model and experimental setup preclude us from investigating the potential role of mesoscale eddy dynamics on the ocean carbon uptake in response to climate change.

Recent literature highlights the potential role of mesoscale eddies in the ocean carbon uptake (Ito et al. 2010) and in water mass formation (Sallée et al. 2011). Besides, a published study (e.g., Farneti and Delworth 2010) has demonstrated that mesoscale eddy dynamics can modulate the transformation of the dense to light water masses in the Southern Ocean in response to climate change. An explicit treatment of the mesoscale activities could alter the response of the water mass carbon uptake to climate change. Since the presence of

active ocean eddy dynamics buffers the oceanic response to atmospheric changes in the regions of the Southern Ocean governed by the influence of the ACC (~<50°S), a weaker response of the IW, DW, and BW could occur. However, the role of the wind-driven Ekman flow, mesoscale eddies, and their interaction is still under debate (e.g., Lovenduski and Ito 2009; Böning et al. 2008). Only high-resolution (i.e., fully eddy resolving) coupled models can be used to address the issues discussed here. Nevertheless, it appears that the mechanisms addressed here act at large spatiotemporal scales and seem to be a robust response of a coarse-resolution ocean biogeochemical model to climate change (e.g., Downes et al. 2009, Lovenduski et al. 2008).

5. Conclusions

By applying a water mass framework, we have characterized the carbon fluxes of the water masses in the Southern Ocean region (<30°S). For each of the water masses, the sensitivities of carbon uptake to rising atmospheric CO_2 and climate change have been determined by applying the methodology of the linear feedback analysis approach of Friedlingstein et al. (2003). This methodology demonstrates that the carbon uptake of the modal and intermediate water masses are highly responsive to rising atmospheric CO_2, while the carbon uptake of the thermocline water masses are highly responsive to change in CO_2 solubility and stratification due to climate change. Because of their strong response to rising atmospheric CO_2, the modal and intermediate water masses control 53% of net cumulative Southern Ocean carbon uptake.

We introduce a new partitioning of the net cumulative carbon uptake, which includes 1) a geochemical component solely due to rising atmospheric CO_2 in absence of climate change; 2) an outcrop surface component, which corresponds to the water mass carbon uptake related to changes in outcrop surface area under a changing climate; and 3) a climate component due to local changes both in CO_2 solubility (owing to change temperature and salinity) and stratification. This new partitioning shows that the outcrop surface component is the dominant fingerprint of climate change on the net cumulative carbon uptake of the Southern Ocean. This component offsets 45% of the cumulative anthropogenic carbon uptake of the Southern Ocean.

Hypotheses on the linear (related mostly to change in water mass outcrop surface area) or nonlinear (owing to changes in marine carbon chemistry, CO_2 solubility, and stratification) responses of the water mass carbon uptake have been proposed. They agree with the conclusions of several previous studies (e.g., Lovenduski and Ito 2009; Tschumi et al. 2008). However, important uncertainties due to the choice of the atmospheric p_{CO_2} scenarios (Gregory et al. 2009; Cadule 2008) and the influence of interior ocean processes (Iudicone et al. 2011) have not been assessed in this work but will be studied in subsequent works. Despite these uncertainties, our analysis suggests that changes in the fractions of the Southern Ocean area occupied by modal, intermediate, and thermocline water masses in response to climate change could cause a reduction in the Southern Ocean carbon uptake.

Finally, we encourage model intercomparisons using the water mass framework, which provides an effective approach to analyze the surface climate-driven changes in carbon uptake of the Southern Ocean. We also suggest that such a water mass framework could provide useful insights into the oceanic climate-induced and carbon-induced sensitivities in the Climate Model Intercomparison Project phase 5.

Acknowledgments. The authors thank C. Le Quéré, M. Lévy, M. Gehlen, J. Orr, and J. Simeon for useful discussion, and also thank anonymous reviewers for helpful comments on the manuscript. The research leading to these results was supported through EU FP7 Project CARBOCHANGE ''Changes in carbon uptake and emissions by oceans in a changing climate,'' which received funding from the European Community's Seventh Framework Program under Grant 264879. This work was made possible thanks to dedicated computers that have been made available by Grand Equipement National de Calcul Intensif (GENCI) at Centre de Calcul Recherche et Technologie (CCRT), Allocation CP1-0040, and the engineer team of IPSL.

REFERENCES

Aumont, O., and L. Bopp, 2006: Globalizing results from ocean in situ iron fertilization studies. *Global Biogeochem. Cycles,* **20,** GB2017, doi:10.1029/2005GB002591.

Barbero, L., J. Boutin, L. Merlivat, N. Martin, T. Takahashi, S. Sutherland, and R. Wanninkhof, 2011: Importance of water mass formation regions for the air-sea CO_2 flux estimate in the Southern Ocean. *Global Biogeochem. Cycles,* **25,** GB1005, doi:10.1029/2010GB003818.

Beckmann, A., and R. Döscher, 1997: A method for improved representation of dense water spreading over topography in geopotential-coordinate models. *J. Phys. Oceanogr.,* **27,** 581–591.

Blanke, B., and P. Delecluse, 1993: Variability of the tropical Atlantic Ocean simulated by a general circulation model with two different mixed-layer physics. *J. Phys. Oceanogr.,* **23,** 1363–1388.

Böning, C. W., A. Dispert, M. Visbeck, S. R. Rintoul, and F. U. Schwarzkopf, 2008: The response of the Antarctic Circumpolar Current to recent climate change. *Nat. Geosci.,* **1,** 864–869, doi:10.1038/ngeo362.

Broecker, W., 1991: The great ocean conveyor. *Oceanography,* **4,** 79–89.

Cadule, P., 2008: Modélisation des interactions entre le système climatique et le cycle du carbone. Ph.D. thesis, University of Paris VI, 375 pp.

Crueger, T., E. Roeckner, T. Raddatz, R. Schnur, and P. Wetzel, 2008: Ocean dynamics determine the response of oceanic CO_2 uptake to climate change. *Climate Dyn.,* **31,** 151–168, doi:10.1007/s00382-007-0342-x.

d'Orgeville, M., W. P. Sijp, M. H. England, and K. J. Meissner, 2010: On the control of glacial-interglacial atmospheric CO_2 variations by the Southern Hemisphere westerlies. *Geophys. Res. Lett.,* **37,** L21703, doi:10.1029/2010GL045261.

Downes, S., N. Bindoff, and S. Rintoul, 2009: Impacts of climate change on the subduction of mode and intermediate water masses in the Southern Ocean. *J. Climate,* **22,** 3289–3302.

Farneti, R., and T. L. Delworth, 2010: The role of mesoscale eddies in the remote oceanic response to altered Southern Hemisphere winds. *J. Phys. Oceanogr.,* **40,** 2348–2354.

Friedlingstein, P., J.-L. Dufresne, P. M. Cox, and P. Rayner, 2003: How positive is the feedback between climate change and the carbon cycle. *Tellus,* **55B,** 692–700, doi:10.1034/j.1600-0889.2003.01461.x.

Gent, P. R., and J. C. McWilliams, 1990: Isopycnal mixing in ocean circulation models. *J. Phys. Oceanogr.,* **20,** 150–155.

González-Dávila, M., J. M. Santana-Casiano, R. A. Fine, J. Happell, B. Delille, and S. Speich, 2011: Carbonate system in the water masses of the southeast Atlantic sector of the Southern Ocean during February and March 2008. *Biogeosciences,* **8,** 1401–1413, doi:10.5194/bg-8-1401-2011.

Gregory, J. M., C. D. Jones, P. Cadule, and P. Friedlingstein, 2009: Quantifying carbon cycle feedbacks. *J. Climate,* **22,** 5232–5250.

Ito, T., M. Woloszyn, and M. Mazloff, 2010: Anthropogenic carbon dioxide transport in the Southern Ocean driven by Ekman flow. *Nature,* **463,** 80–83, doi:10.1038/nature08687.

Iudicone, D., G. Madec, and T. J. McDougall, 2008: Water-mass transformations in a neutral density framework and the key role of light penetration. *J. Phys. Oceanogr.,* **38,** 1357–1376.

——, K. B. Rodgers, I. Stendardo, O. Aumont, G. Madec, L. Bopp, O. Mangoni, and M. Ribera d'Alcala, 2011: Water masses as a unifying framework for understanding the Southern Ocean carbon cycle. *Biogeosciences,* **8,** 1031–1052, doi:10.5194/bg-8-1031-2011.

Jackett, D. R., and T. J. McDougall, 1997: A neutral density variable for the world's oceans. *J. Phys. Oceanogr.,* **27,** 237–263.

Lenton, A., and R. J. Matear, 2007: Role of the southern annular mode (SAM) in Southern Ocean CO_2 uptake. *Global Biogeochem. Cycles,* **21,** GB2016, doi:10.1029/2006GB002714.

——, F. Codron, L. Bopp, N. Metzl, P. Cadule, A. Tagliabue, and J. Le Sommer, 2009: Stratospheric ozone depletion reduces ocean carbon uptake and enhances ocean acidification. *Geophys. Res. Lett.,* **36,** L12606, doi:10.1029/2009GL038227.

Le Quéré, C., and Coauthors, 2007: Saturation of the Southern Ocean CO_2 sink due to recent climate change. *Science,* **316,** 1735–1738, doi:10.1126/science.1136188.

——, and Coauthors, 2009: Trends in the sources and sinks of carbon dioxide. *Nat. Geosci.,* **2,** 831–836, doi:10.1038/ngeo689.

Lovenduski, N. S., and T. Ito, 2009: The future evolution of the Southern Ocean CO_2 sink. *J. Mar. Res.,* **67,** 597–617, doi:10.1357/002224009791218832.

——, N. Gruber, and S. C. Doney, 2008: Toward a mechanistic understanding of the decadal trends in the Southern Ocean carbon sink. *Global Biogeochem. Cycles,* **22,** GB3016, doi:10.1029/2007GB003139.

Madec, G., 2008: NEMO ocean engine. IPSL Note du Pole de Modélisation 27, 321 pp.

Marinov, I., and A. Gnanadesikan, 2011: Changes in ocean circulation and carbon storage are decoupled from air-sea CO_2 fluxes. *Biogeosciences,* **8,** 505–513, doi:10.5194/bg-8-505-2011.

——, M. Follows, A. Gnanadesikan, J. L. Sarmiento, and R. D. Slater, 2008a: How does ocean biology affect atmospheric pCO_2? Theory and models. *J. Geophys. Res.,* **113,** C07032, doi:10.1029/2007JC004598.

——, A. Gnanadesikan, J. L. Sarmiento, J. R. Toggweiler, M. Follows, and B. K. Mignone, 2008b: Impact of oceanic circulation on biological carbon storage in the ocean and atmospheric pCO_2. *Global Biogeochem. Cycles,* **22,** GB3007, doi:10.1029/2007GB002958.

Marti, O., and Coauthors, 2010: Key features of the IPSL ocean atmosphere model and its sensitivity to atmospheric resolution. *Climate Dyn.,* **34,** 1–26, doi:10.1007/s00382-009-0640-6.

Mikalhof-Fletcher, S. E., and Coauthors, 2007: Inverse estimates of the oceanic sources and sinks of natural CO_2 and the implied oceanic carbon transport. *Global Biogeochem. Cycles,* **21,** GB1010, doi:10.1029/2006GB002751.

Murnane, R., J. L. Sarmiento, and C. Le Quéré, 1999: Spatial distribution of air-sea CO_2 fluxes and the interhemispheric transport of carbon by the oceans. *Global Biogeochem. Cycles,* **13,** 287–305.

Orsi, A. H., G. C. Johnson, and J. L. Bullister, 1999: Circulation, mixing, and production of Antarctic Bottom Water. *Prog. Oceanogr.,* **43,** 55–109, doi:10.1016/S0079-6611(99)00004-X.

Roy, T., and Coauthors, 2011: Regional impacts of climate change and atmospheric CO_2 on future ocean carbon uptake: A multimodel linear feedback analysis. *J. Climate,* **24,** 2300–2318.

Sabine, C. L., and Coauthors, 2004: The oceanic sink for anthropogenic CO_2. *Science,* **305,** 367–371, doi:10.1126/science.1097403.

Sallée, J.-B., K. Speer, S. Rintoul, and S. Wijffels, 2011: Southern Ocean thermocline ventilation. *J. Phys. Oceanogr.,* **40,** 509–529.

Sarmiento, J. L., and N. Gruber, 2006: *Ocean Biogeochemical Dynamics*. Princeton University Press, 503 pp.

——, P. Monfray, E. Maier-Reimer, O. Aumont, R. J. Murnane, and J. C. Orr, 2000: Sea-air CO_2 fluxes and carbon transport: A comparison of three ocean general circulation models. *Global Biogeochem. Cycles,* **14,** 1267–1281.

——, N. Gruber, M. A. Brzezinski, and J. P. Dunne, 2004: High-latitude controls of thermocline nutrients and low latitude biological productivity. *Nature,* **479,** 556, doi:10.1038/nature10605.

Sloyan, B., and S. Rintoul, 2001: The Southern Ocean limb of the global deep overturning circulation. *J. Phys. Oceanogr.,* **31,** 143–173.

Sørensen, J., J. Ribbe, and G. Shaffer, 2001: Antarctic Intermediate Water mass formation in ocean general circulation models. *J. Phys. Oceanogr.,* **31,** 3295–3311.

Taylor, K. E., R. J. Stouffer, and G. A. Meehl, 2012: An overview of CMIP5 and the experiment design. *Bull. Amer. Meteor. Soc.,* **93,** 485–498.

Tjiputra, J. F., K. Assmann, M. Bentsen, I. Bethke, O. H. Otterå, C. Sturm, and C. Heinze, 2010: Bergen earth system model (BCM-C): Model description and regional climate-carbon cycle feedbacks assessment. *Geosci. Model Dev.,* **3,** 123–141, doi:10.5194/gmd-3-123-2010.

Toggweiler, J. R., J. L. Russell, and S. R. Carson, 2006: Midlatitude westerlies, atmospheric CO_2, and climate change during

the ice ages. *Paleoceanography,* **21,** PA2005, doi:10.1029/2005PA001154.

Tomczak, M., and S. Liefrink, 2005: Interannual variations of water mass volumes in the Southern Ocean. *J. Atmos. Ocean Sci.,* **10,** 31–42.

Treguier, A. M., I. M. Held, and V. D. Larichev, 1997: Parameterization of quasigeostrophic eddies in primitive equation ocean models. *J. Phys. Oceanogr.,* **27,** 567–580.

Tschumi, T., F. Joos, and P. Parekh, 2008: How important are Southern Hemisphere wind changes for low glacial carbon dioxide? A model study. *Paleoceanography,* **23,** PA4208, doi:10.1029/2008PA001592.

Verdy, A., S. Dutkiewicz, M. J. Follows, J. Marshall, and A. Czaja, 2007: Carbon dioxide and oxygen fluxes in the Southern Ocean: Mechanisms of interannual variability. *Global Biogeochem. Cycles,* **21,** GB2020, doi:10.1029/2006GB002916.

Yoshikawa, C., M. Kawamiya, T. Kato, Y. Yamanaka, and T. Matsuno, 2008: Geographical distribution of the feedback between future climate change and the carbon cycle. *J. Geophys. Res.,* **113,** G03002, doi:10.1029/2007JG000570.